Dalton Transactions

Dendritic CdS assemblies for removal of organic dye molecules†

Zhou Yu, Fengyu Qu* and Xiang Wu*

In this paper, novel CdS 3D assemblies are prepared *via* a facile and effective hydrothermal route using dimethyl sulfoxide as the growth template. Morphologies, microstructures and photocatalytic properties of the as-synthesized products are investigated in detail. It was found that dimethyl sulfoxide played an important role in the formation of CdS assemblies. A possible growth mechanism for CdS assemblies was proposed based on the experimental results. In addition, CdS assemblies exhibit superior photocatalytic activities by the photodegradation of eosin B, Methyl orange (MO) and Rhodamine B (RhB) under visible light irradiation, with a comparison with other CdS nanostructures, P25 and α-Fe$_2$O$_3$ powders, demonstrating potential applications in removal of organic dye molecules from waste water.

1 Introduction

Nowadays, environmental pollution and destruction on a global scale are attracting increasing attention.[1–5] For the sustainable development of human society, to develop both pollution-free technologies for environmental remediation and alternative clean energy supplies is an urgent task.[6] Semiconductor photocatalysis can provide a simple way to induce degradation of organic pollutants by UV/Vis light irradiation.[7–11] It can be expected that novel micro/nanostructures are beneficial to efficient photocatalytic degradation of organic pollutants from waste water.

So far, ZnO, TiO$_2$ and SnO$_2$ have been regarded as efficient photocatalysts due to their high catalytic activities, great stabilities, nontoxicity and low cost, but the wide bandgaps hindered their sufficient utilization of sunlight.[11–19] As an important II–VI semiconductor, CdS is regarded as one of the most attractive visible light-driven photocatalysts due to its relatively narrow band gap of 2.42 eV that corresponds well with the solar spectrum.[20–28] It is well-known that nanomaterials' properties greatly depend on their morphological features. Therefore, a great deal of effort has been devoted to preparing CdS nanomaterials with the desired size and architecture through various methods. For example, Gao and co-workers synthesized three dimensional CdS nanocrystals using hexamethylenetetramine [(CH$_2$)$_4$N$_4$, HMT] as a capping reagent.[29]

Key Laboratory for Photonic and Electronic Bandgap Materials, Ministry of Education and College of Chemistry and Chemical Engineering, Harbin Normal University, Harbin 150025, P. R. China. E-mail: wuxiang05@gmail.com, qufengyu@hrbnu.edu.cn

†Electronic supplementary information (ESI) available. See DOI: 10.1039/c3dt53256a

Yu *et al.* reported a solvothermal approach to synthesize urchin-like CdS flowers and branched nanowires.[23] In our previous report, we obtained dendrite-like CdS hierarchical nanostructures by a facile and effective hydrothermal route at a mild temperature.[30] Although several preparation methods have been proposed to fabricate CdS nanomaterials, to develop synthetic strategies for CdS nanocrystals with various morphologies is still a great challenge.

Herein, we prepared successfully a kind of novel 3D CdS assembly with a unique spatial architecture *via* a simple one-step hydrothermal route using dimethyl sulfoxide (DMSO) as the growth template. A possible growth mechanism of the as-prepared CdS products is proposed. The photocatalytic performances of the as-obtained CdS products for the photodegradation of organic dyes under visual light irradiation were investigated in detail. The results showed that the as-synthesized 3D CdS assemblies possess superior photodegradation activities toward organic dyes molecules.

2 Experimental

All reagents were of an analytical grade and used without further purification. In a typical procedure, 1 mmol CdCl$_2$·5H$_2$O, 3 mmol thiourea (CH$_4$N$_2$O$_4$S) and 0.2 ml DMSO were dissolved into 40 ml deionized water in sequence to form a homogeneous solution with constant stirring. After stirring for 30 min, the suspension was transferred into a Teflon-lined stainless steel autoclave with a capacity of 50 ml. The autoclave was sealed and heated in a program-controlled oven at 160 °C for 10 h. After the system was cooled naturally to room temperature, the precipitates obtained was washed several times

with deionized water and ethanol, and then dried in a vacuum at 60 °C for 10 h.

The phase and composite of the as-obtained product were characterized by X-ray diffraction (XRD, Rigaku Dmax-rB, Cu Kα radiation, λ = 0.1542 nm 40 kV, 100 mA). The morphology and microstructure of the samples were characterized with a scanning electron microscope (SEM, Hitachi-4800), a transmission electron microscope (TEM, JEOL 2010EX) and Raman spectroscopy (HR800). A specific surface area analyzer (NOVA2000E) was used to measure the N_2-sorption isotherm. The Brunauer–Emmett–Teller (BET) formula was further used to calculate the specific surface area. The photocatalytic degradation activities were investigated by monitoring dye decolorization at the maximum absorption wavelength, using a UV/Vis spectrometer (Shimazu UV-2550).

The evaluation of photocatalytic performance of the as-synthesized samples for photocatalytic decomposition or removal of eosin B, Methyl Orange (MO) and Rhodamine B (RhB) aqueous solution was performed as follows: 0.05 g CdS assemblies were suspended in 200 ml organic dyes aqueous solution (10 mg L^{-1}). The suspensions were magnetically stirred in the dark for 60 min to ensure an adsorption/desorption equilibrium of organic dye aqueous solution, and the solution was then exposed to an 800 W xenon lamp at room temperature. At given irradiation intervals, a series of aqueous solution was collected for analysis. The photocatalytic performance of the catalyst was evaluated by monitoring the visible absorbance characteristic of the targeted organic dye molecules using UV/Vis spectroscopy. The changes in organic dye concentration under xenon lamp irradiation were calculated as follows:

$$I = C/C_0 \times 100\%$$

where C_0 and C are the equilibrium concentration of organic dyes before and after irradiation, respectively. Photocatalytic activity derived from the change in organic dye concentration can be represented by the relative ratio C/C_0.

3 Results and discussion

The morphology and microstructural details of the as-prepared 3D CdS assemblies are investigated by SEM and TEM observation. Fig. 1a presents the overall morphology of the as-synthesized CdS assemblies, clearly observing that the product exhibits 3D assemblies microstructure with the diameter of 4–7 μm. Fig. 1b shows single CdS 3D assemblies consisting of quantities of dendrites. Each of them is composed of a central trunk with a length of 3–4 μm and numerous branches with an average length of 500 nm, which are distributed in parallel in the central trunk. Single TEM image of CdS 3D assemblies shown in Fig. 1c also confirmed the observations from SEM. The SAED pattern taken from the trunk tip and branch tip were observed to be exactly the same, and the diffraction spots demonstrate that the entire leaf is a CdS single crystal oriented
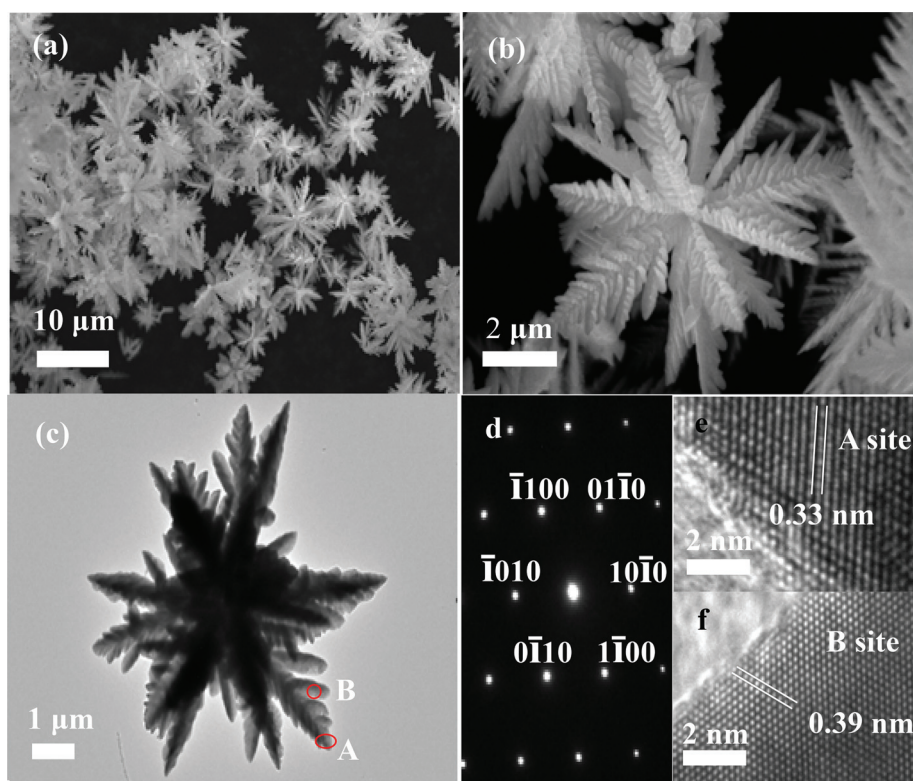

Fig. 1 Morphologies of the as synthesized CdS 3D assemblies. (a–b) SEM images at different magnification. (c) TEM image of a single microstructure; (d) selected-area electron diffraction (SAED) pattern of the as-synthesized products. (e) and (f) HRTEM image.
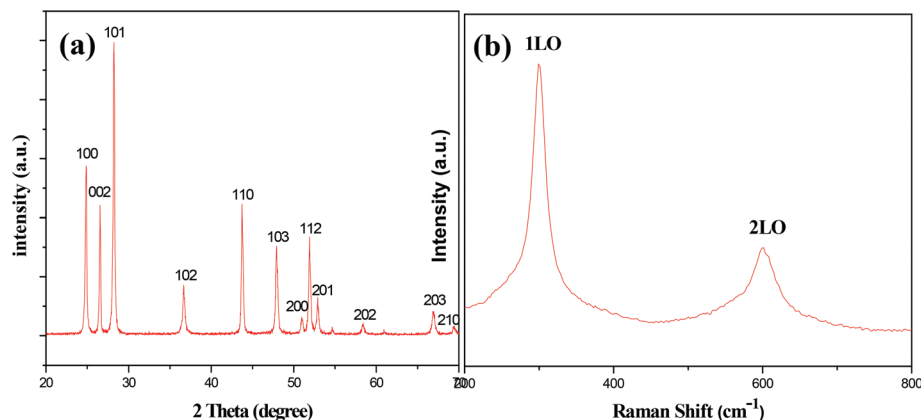
Fig. 2 (a) XRD pattern of the as-synthesized products, (b) Raman spectrum of the as-synthesized products.

along [0001] with the three branches along [10$\bar{1}$0], [1$\bar{1}$00], and [0$\bar{1}$10], respectively (see Fig. 1d). Fig. 1e and f are HRTEM images taken from the areas labeled A and B in Fig. 1c. The lattice spacing of 0.39 nm and 0.33 nm correspond to the distance between two {10$\bar{1}$0} crystal planes and [0001] crystal planes.

Fig. 2a shows a representative XRD pattern of the as-prepared product, all diffraction peaks can be indexed to hexagonal wurtzite CdS (JCPDS no. 41-1049). No obvious diffraction peaks from other impurities were observed, suggesting high crystallinity of CdS 3D assemblies. Raman scattering spectroscopy was also performed to further study the structures of CdS product. Fig. 2b displays room temperature Raman spectrum of CdS microstructures. Two Raman peaks centered at 301 and 602 cm^{-1} are observed. They can be assigned to the first and second order longitudinal optical (LO) phonon modes of CdS, respectively.[31,32] The ratio of 2LO mode intensity to 1LO mode intensity, which reflects exciton–photon coupling, was calculated to be 0.48, the ratio is known to decrease in the particle size of CdS.[33,34] The symmetric and sharp peaks of CdS products suggest that CdS 3D assemblies structures are highly crystalline, which is consistent with the XRD results.

Nitrogen adsorption–desorption measurements were conducted to determine the specific surface area and pore size of the CdS 3D assemblies structures. The nitrogen adsorption–desorption isotherm and the corresponding BJH pore diameter distribution of CdS 3D assemblies are presented in Fig. 3. It reveals that the isotherm of the as-synthesized CdS product is a type IV isotherm with H$_3$-type hysteresis loops according to IUPAC. Quantitative calculation demonstrates that the as-prepared CdS product possesses a BET surface area of 18.276 m^2 g^{-1}.

To better understand the formation of CdS 3D assemblies, a series of controlled experiments were conducted by varying the experimental parameters. At first, time dependent SEM images of the as-synthesized products were investigated, as shown in Fig. S1†. In Fig. S1a†, at the early stage of the reaction, irregular small particles with the average size of 200 nm
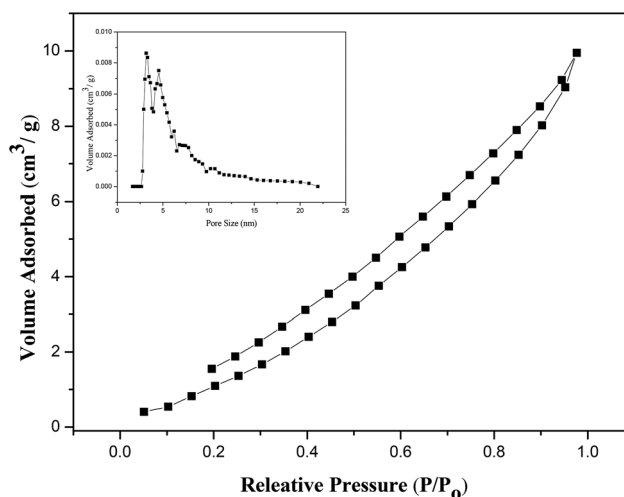

Fig. 3 Nitrogen adsorption/desorption isotherm and pore diameter distribution of the as-synthesized samples.

aggregate for 0.5 h. With a prolonged time up to 1 h (Fig. S1b†), some sheet-like structures through a "back-to-back" way assemble together to form an original parent structure. From this stage, further growth of each sheet would be overwhelmed during formation process of the final product. When the reaction time is increased to 3 h, the sheets partially split and changed to dendrite structures (Fig. S1c†). After reaction of 5 h, the branch-like structure of the dendrite outspread gradually (see in Fig. S1d†). From Fig. S1e†, on further increasing the reaction time to 8 h the branches of the dendrites became larger. The hierarchical structure almost did not change significantly when the reaction time was further increased to 10 h (Fig. S1f†), revealing extension of reaction times can just affect the size of the as-prepared products.

Fig. S2† shows the as-synthesized products in the presence of different quantities of DMSO at 160 °C for 10 h. It can be found that without using DMSO the as-obtained products show a dendritic-like structure with a pronounced trunk and highly ordered branches distributed on both sides of the
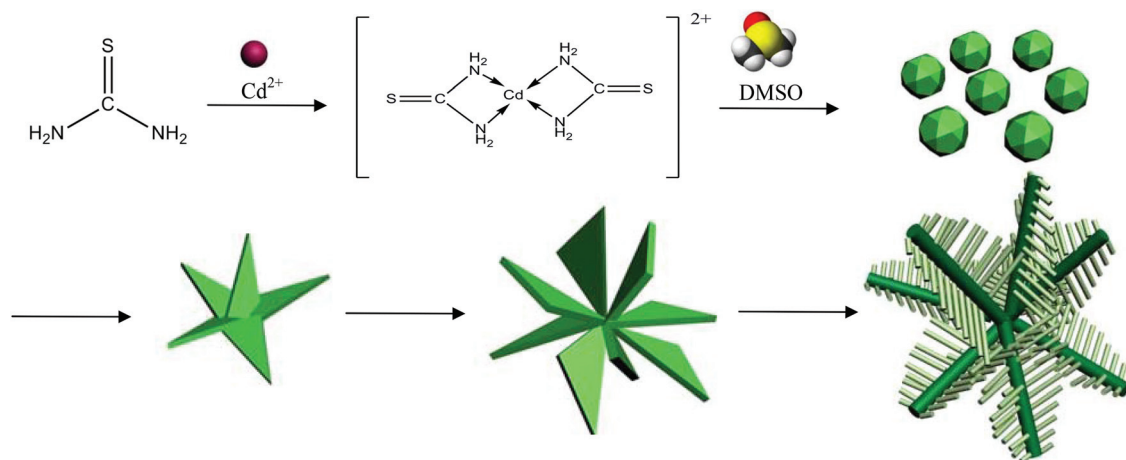
Paper

Dalton Transactions

Fig. 4 Growth schematic of the as-synthesized CdS 3D assemblies.

trunk, as shown in Fig. S2a†. It is noteworthy that such dendritic-like structures did not assemble together, showing that DMSO plays a significant role for the growth of a dendritic-like structure assembly. When the addition of DMSO was 0.1 ml, the samples exhibited a smaller size (Fig. S2b†) compared with that when the addition was 0.2 ml (Fig. S2c†). On further increasing the dosage of DMSO to 0.3 ml (seen from Fig. S2d†), the sizes of branches became irregular.

Based on the above experimental results, a possible growth mechanism of CdS 3D assemblies may be proposed as follows: at the initial stage, the Cd^{2+} and the thiourea might form the complex compound (Cd–thiourea) because of the strong coordinating capacity of thiourea. Then, the Cd–thiourea complex tends to decompose to release the active Cd^{2+} and S^{2-} gradually with increase in temperature.[35] At the same time, the DMSO molecules as the surfactant assembly form an arc-like structure in solution, the methyl groups in the molecules of DMSO would be in the interior because of their hydrophobic property, while the S=O group will be at the exterior. The released S^{2-} ions react with the Cd^{2+} ions which are coordinated on the DMSO templates, resulting in the formation of the growth nuclei. With an increase of reaction time, primary nuclei gradually form the sheet-like structure. The sheet-like CdS nanostructures grow fast along certain directions due to anisotropic characteristics.[36–39] Fig. 4 showed the growth schematic diagram of CdS assemblies.

UV-vis diffuse reflectance spectrum was used to investigate the light absorption property of the as-synthesized CdS 3D assemblies. In Fig. 5, CdS 3D assemblies exhibit a steep absorption edge located at 548 nm, indicating the sample possesses a visible light absorption band, which endows it potential applications in solar catalysis. In comparison to pure eosin B dye molecules, the absorption edge of CdS 3D assemblies with eosin B exhibit a wide visible light absorption band, which could be attributed to the presence of CdS 3D assemblies as visible-light sensitization, which has a strong and wide absorption band in the visible-light region.
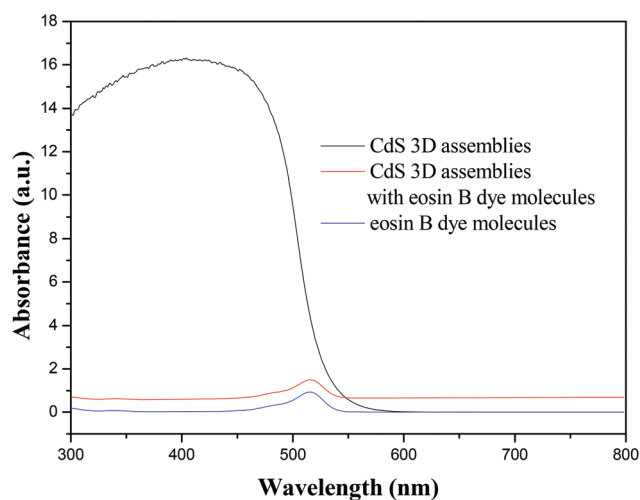

Fig. 5 UV-Vis diffuse reflection spectra of the as-synthesized CdS 3D assemblies.

To demonstrate potential applications of the as-synthesized CdS 3D assemblies in waste water treatment, photocatalytic activities of the as-obtained products in the degradation of eosin B, RhB and MO dyes were investigated in detail. Absorption spectra of photodegradation of different dyes under visual light irradiation are shown in Fig. 6. Fig. 6a shows the UV/Vis adsorption spectra of eosin B solution in the presence of CdS 3D assemblies under visual light at different time intervals. The main absorption peak of eosin B centered at 517 nm before and after irradiation. When the light was turned on, the main peaks decreased continuously with increased irradiation time, indicating that the eosin B solution was decomposed in the present system. The intensity of the absorbance peaks drops rapidly with the elongation of the exposure time and completely disappears after about 80 min, the efficiency is up to 98.7%. Similar photodegradation experiments were also conducted to other target molecules. Fig. 6b shows the
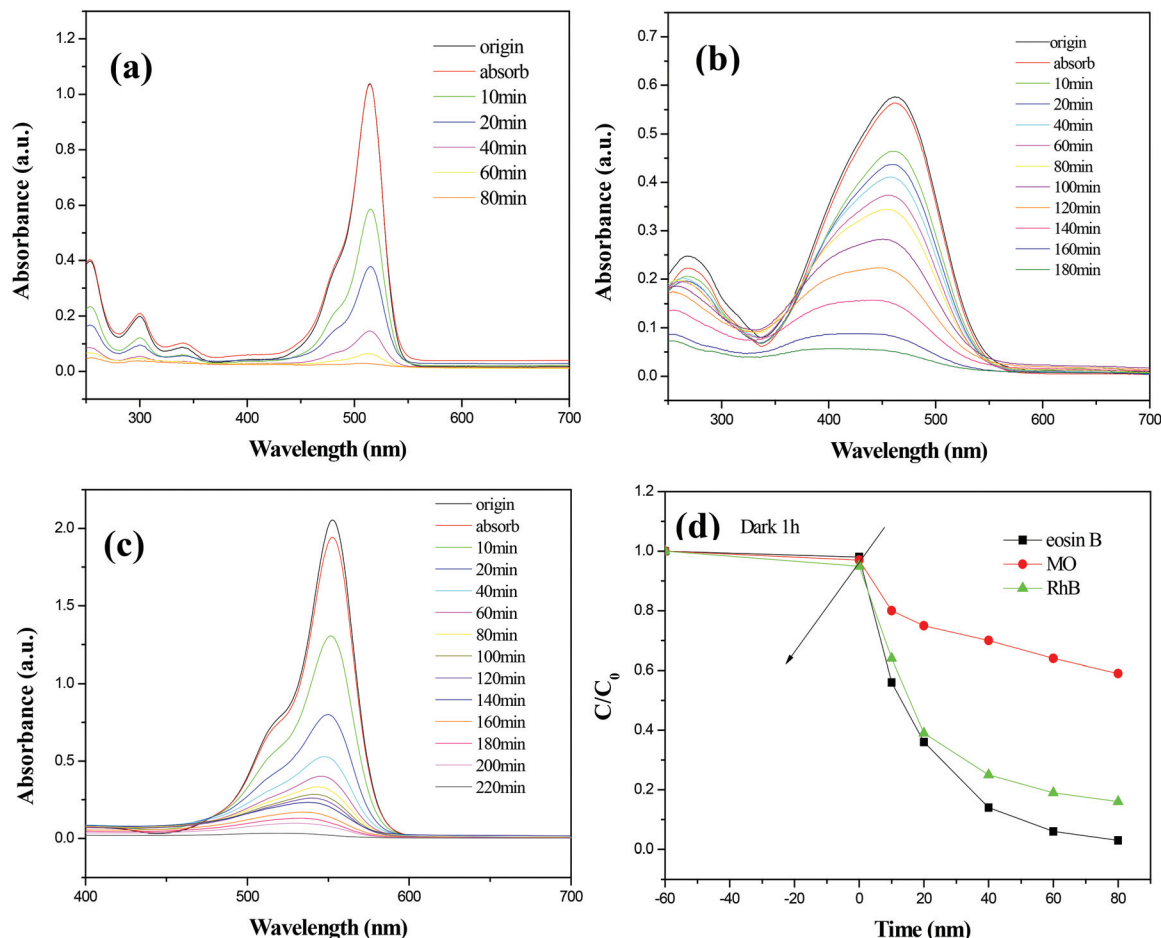
Fig. 6 Variations in adsorption spectra of organic dye solution in the presence of the CdS 3D assemblies irradiated by a visible lamp for different time periods: (a) eosin B, (b) Methyl orange, (c) Rhodamine B, (d) photocatalysis degradation rate of eosin B, Methyl orange and Rhodamine B.

absorption spectra of MO aqueous solution for various irradiation durations. When the illumination time was extended to 180 min, the color of the MO solution vanished. The absorption peak corresponding to MO at 465 nm diminished gradually and the photocatalytic degradation rate of MO was 92%. For further comparison, the photocatalytic degradation rates of RhB with CdS 3D assemblies were shown in Fig. 6c. The absorption peak corresponding to RhB is located at 553 nm, and nearly 98% of RhB molecules were decomposed after 220 min. Fig. 6d illustrates a comparison of the degradation rates of the above three dyes under the same condition. It is found that the degradation ratio of eosin B is better than the other two dyes when the irradiation time reaches 80 min.

To further evaluate the degradation capability to eosin B solution with different photocatalysts, dendritic-like CdS, commercial CdS powders, P25 and α-Fe$_2$O$_3$ powders were chosen for comparison. Fig. 7a–e correspond to the adsorption spectra of eosin B solution in the presence of CdS 3D assemblies, dendritic-like CdS, commercial CdS powders, a-Fe$_2$O$_3$ powders and P25 under visual light at regular intervals. Fig. 7f reveals the photocatalytic degradation ratio of eosin B using several

different photocatalysts under the same conditions. After irradiation for 80 min, about 92% of eosin B decomposes in the case of dendritic-like CdS as the catalyst (red curve in Fig. 7f) and about 84% of decolorization for commercial CdS powders (blue curve). The green curve also indicates that the poor photocatalytic performance of 46% in the case of P$_{25}$. Among various semiconductors, a-Fe$_2$O$_3$ is also regarded as one of the most attractive visible light-driven photocatalysts. For comparison, the photocatalytic activities of a-Fe$_2$O$_3$ powders under xenon lamp irradiation have also been tested. It is found that α-Fe$_2$O$_3$ powders degradation rate is only 17% (pink curve). In the absence of xenon light illumination on eosin B there is only 10% degradation of the dye (yellow curve in Fig. 7f), indicating that eosin B degradation needs an electron-transfer mediator under visible light. As for CdS 3D assemblies, the degradation rate is 97% after 80 min illumination (black curve), which is evidently greater than that of the above photocatalysts. Hence, the order of the decomposition rate of eosin B aqueous solution in the presence of the above catalysts is as follows: CdS 3D assemblies (97%) > dendritic-like CdS (92%) > commercial CdS powders (84%) > P25 (46%) > α-Fe$_2$O$_3$ powders (17%) > blank experiment (10%). The
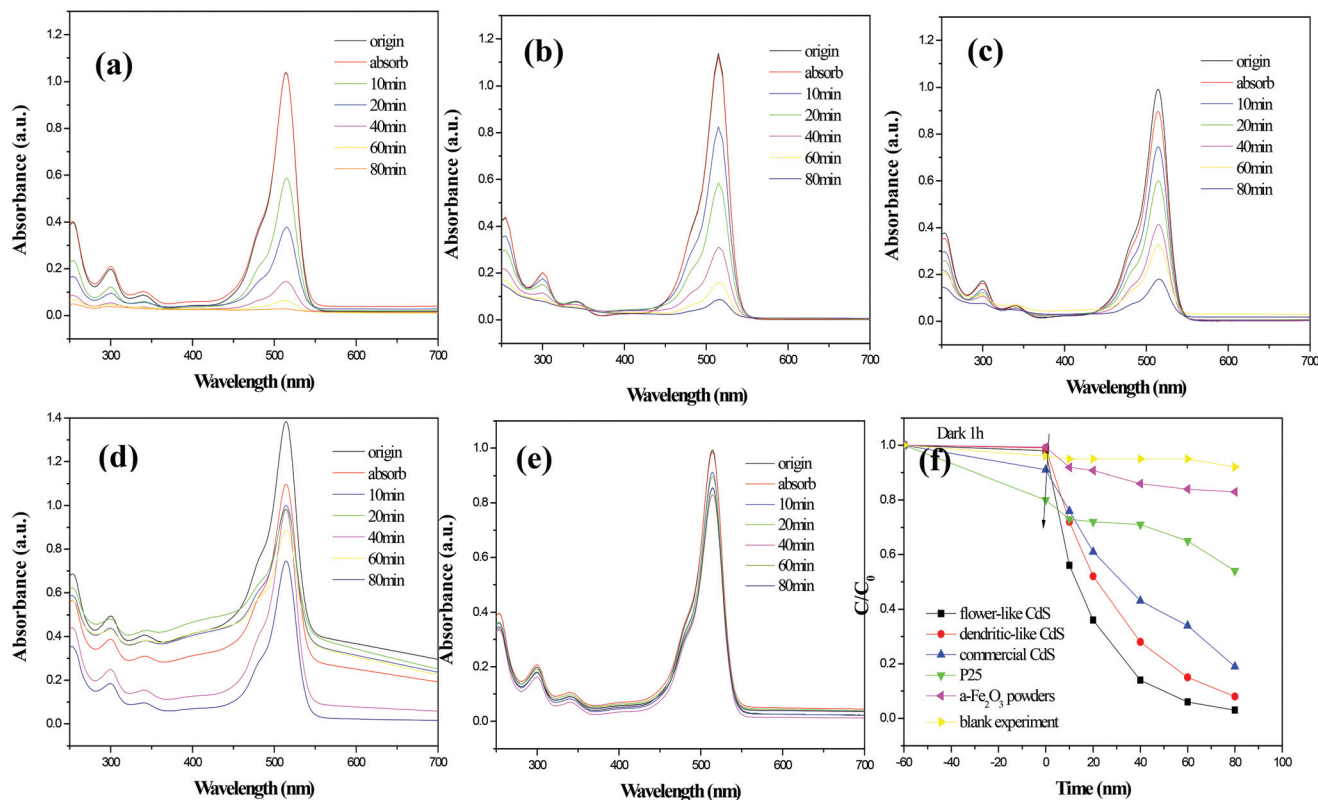
Fig. 7 Adsorption spectra of eosin red solution in the presence of: (a) CdS 3D assemblies, (b) dendritic-like CdS, (c) commercial CdS powders, (d) P25, (e) a-Fe₂O₃ powders, (f) photocatalytic degradation ratio of eosin B using several different photocatalysts under the same conditions.

superior photocatalytic efficiencies of CdS 3D assemblies may be attributed to their unique spatial structures, large surface area and high crystallinity.[40,41] It indicates that such CdS 3D assemblies may have potential applications in eliminating organic pollutants in waste water.

It is well-known that the photocatalytic oxidation of organic pollutants obeys Langmuir–Hinshelwood kinetics.[42] This kind of pseudo-first-order kinetics can be represented as follows:

$$r = -\mathrm{d}C/\mathrm{d}t = -k'KC/1 + KC \qquad (1)$$

where r is the rate of dye mineralization, k' is the rate constant, C is the dye concentration, and K is the adsorption coefficient. By integration, eqn (1) can be arranged into the following:

$$\ln C/C_0 = -kt \qquad (2)$$

where C_0 is the initial concentration of the eosin B solution and k is a rate constant. According to eqn (2), rate constant k can be given by the slope of fitting curves, when plotting $\ln(C/C_0)$ against. The degradation data with the linear fitting curves are plotted in Fig. 8. The reaction rate constants for CdS 3D assemblies, dendritic-like CdS, commercial CdS powders, P25, α-Fe₂O₃ powders and blank experiment are 0.04562 min⁻¹, 0.03212 min⁻¹, 0.02100 min⁻¹, 0.00775 min⁻¹, 0.00182 min⁻¹, and 0.00125 min⁻¹ respectively. The results illustrate that CdS 3D assemblies possess excellent photocatalytic properties compared with other photocatalysts under visible light irradiation.
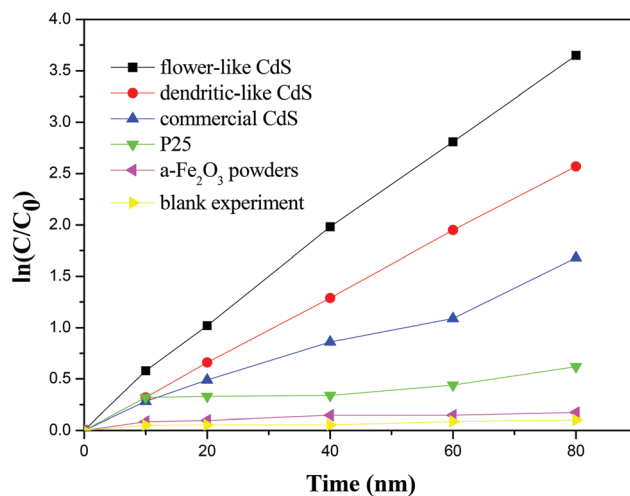

Fig. 8 The linear fitting of the photocatalytic activity.

4   Conclusions

In summary, novel CdS 3D assemblies were prepared *via* a facile hydrothermal route using DMSO as the growth template. The possible growth mechanism of CdS 3D assemblies was proposed based on the experimental results. The photocatalytic degradation experiments showed that the CdS 3D assemblies exhibit higher photocatalytic activity compared

with dendritic-like CdS, commercial CdS powders, P25 and a-Fe$_2$O$_3$ powders. The improved photocatalyst efficiency of CdS 3D assemblies may have potential application in industrial waste water treatment.

Acknowledgements

Notes and references

1 J. A. Lee, K. C. Krogman, M. Ma, R. M. Hill, P. T. Hammond and G. C. Rutledge, *Adv. Mater.*, 2008, **20**, 1252.
2 J. Z. Yang, J. W. Yu, J. Fan, D. P. Sun, W. H. Tang and X. J. Yang, *J. Hazard. Mater.*, 2011, **189**, 377.
3 W. N. Jia, B. X. Jia, X. Wu, F. Y. Qu and H. J. Fan, *Sci. Adv. Mater.*, 2013, **5**, 1329.
4 J. Wang, F. Y. Qu and X. Wu, *Mater. Express*, 2013, **3**, 256.
5 J. Wang, F. Y. Qu and X. Wu, *Sci. Adv. Mater.*, 2013, **5**, 1052.
6 H. Tong, S. X. Ouyang, Y. P. Bi, N. Umezawa, M. Oshikiri and J. H. Ye, *Adv. Mater.*, 2012, **24**, 229.
7 M. D. Hernandez-Alonso, F. Fresno, S. Suarez and J. M. Coronado, *Energy Environ. Sci.*, 2009, **2**, 1231.
8 B. X. Jia, W. N. Jia, X. Wu and F. Y. Qu, *Sci. Adv. Mater.*, 2012, **4**, 1127.
9 M. N. Liu, H. X. Wang, C. Yan and J. Bell, *Mater. Focus*, 2012, **1**, 136.
10 S. Y. Song and H. J. Zhang, *Rev. Adv. Sci. Eng.*, 2012, **1**, 165.
11 J. Ma, L. S. Qiang, H. Y. Li and X. B. Tang, *Sci. Adv. Mater.*, 2012, **4**, 1185.
12 X. Chen and S. S. Mao, *Chem. Rev.*, 2007, **107**, 2891.
13 H. Zhang and Y. F. Zhu, *J. Phys. Chem. C*, 2010, **114**, 5822.
14 F. H. Chu, C. W. Huang, C. L. Hsin, C. W. Wang, S. Y. Yu, P. H. Yeh and W. W. Wu, *Nanoscale*, 2012, **4**, 1471.
15 Y. K. Lai, L. Sun, Y. C. Chen, H. F. Zhuang, C. J. Lin and J. W. Chen, *J. Electrochem. Soc.*, 2006, **153**, 123.
16 Y. T. Han, X. Wu, Y. L. Ma, L. H. Gong, F. Y. Qu and H. J. Fan, *CrystEngComm*, 2011, **13**, 3506.
17 Q. F. Zhang, T. P. Chou, B. Russo, S. A. Jenekhe and G. Z. Cao, *Angew. Chem., Int. Ed.*, 2008, **47**, 2402.
18 B. X. Jia, W. N. Jia, Y. L. Ma, X. Wu and F. Y. Qu, *Sci. Adv. Mater.*, 2012, **4**, 702.
19 W. N. Jia, B. X. Jia, X. Wu and F. Y. Qu, *CrystEngComm*, 2012, **14**, 7759.
20 X. S. Fang, T. Y. Zhai, U. K. Gautam, L. Li, L. M. Wu, Y. Bando and D. Golberg, *Prog. Mater. Sci.*, 2011, **56**, 175.
21 L. F. Hu, J. Yan, M. Y. Liao, H. J. Xiang, X. G. Gong, L. D. Zhang and X. S. Fang, *Adv. Mater.*, 2012, **24**, 2305.
22 G. Dukovic, M. G. Merkle, J. H. Nelson, S. M. Hughes and A. P. Alivisatos, *Adv. Mater.*, 2008, **22**, 4036.
23 W. T. Yao, S. H. Yu, S. J. Liu, J. P. Chen, X. M. Liu and F. Q. Li, *J. Phys. Chem. B*, 2006, **110**, 11704.
24 Z. A. Peng and X. G. Peng, *J. Am. Chem. Soc.*, 2001, **123**, 183.
25 L. Dong, T. Gushtyuk and J. Jiao, *J. Phys. Chem. B*, 2004, **108**, 1617.
26 L. D. Nyamen, V. S. R. R. Pullabhotla, A. A. Nejo, P. T. Ndifon, J. H. Warner and N. Revaprasadu, *Dalton Trans.*, 2012, **41**, 8297.
27 B. J. S. Johnson, J. H. Wolf and A. S. Zalusky, *Chem. Mater.*, 2004, **16**, 2909.
28 Y. Guo, J. Wang, Z. K. Tao, F. F. Dong, K. Wang, X. M. Ma, P. H. Yang, P. P. Hu, Y. T. Xu and L. Yang, *CrystEngComm*, 2012, **14**, 1185.
29 F. Gao, Q. Y. Lu, X. K. Meng and S. Komarneni, *J. Phys. Chem. C*, 2008, **112**, 13359.
30 Z. Yu, X. Wu, J. Wang, W. N. Jia, G. S. Zhu and F. Y. Qu, *Dalton Trans.*, 2013, **42**, 4633.
31 G. Z. Shen and C. J. Lee, *Cryst. Growth Des.*, 2005, **5**, 1085.
32 S. Kar and S. Chaudhuri, *J. Phys. Chem. B*, 2006, **110**, 4542.
33 T. Y. Zhai, X. S. Fang, Y. Bando, B. Dierre, B. D. Liu, H. B. Zeng, X. J. Xu, Y. Huang, X. L. Yuan, T. Sekiguchi and D. Golberg, *Adv. Funct. Mater.*, 2009, **19**, 2423.
34 M. R. Kim and D. J. Jang, *Chem. Commun.*, 2008, 5218.
35 L. Zeiri, I. Patla, S. Acharya, Y. Golan and S. Efrima, *J. Phys. Chem. C*, 2007, **111**, 11843.
36 Y. M. Guo, J. F. Wang, L. Yang, J. Zhang, K. Jiang, W. J. Li, L. L. Wang and L. L. Jiang, *CrystEngComm*, 2011, **13**, 5045.
37 M. Darko and D. Miha, *Cryst. Growth Des.*, 2008, **8**, 2182.
38 X. B. He and L. Gao, *J. Phys. Chem. C*, 2009, **113**, 10981.
39 S. R. Aghdaee and V. Soleimanian, *J. Cryst. Growth*, 2012, **341**, 66.
40 H. B. Zeng, W. P. Cai, P. S. Liu, X. X. Xu, H. J. Zhou, C. Klingshirn and H. Kalt, *ACS Nano*, 2008, **2**, 1661.
41 H. B. Zeng, G. T. Duan, Y. Li, S. K. Yang, X. X. Xu and W. P. Cai, *Adv. Funct. Mater.*, 2010, **20**, 561.
42 R. K. Wahi, W. W. Yu, Y. P. Liu, M. L. Mejia, J. C. Falkner, W. Nolte and V. L. Colvin, *J. Mol. Catal. A: Chem.*, 2005, **242**, 48.